Inorg. Chem. **2004**, *43*, 5919–5930

Mixed-Valence $Mn^{III}Mn^{IV}$ Clusters $[Mn_7O_8(O_2SePh)_8(O_2CMe)(H_2O)]$ and $[Mn_7O_8(O_2SePh)_9(H_2O)]$: Single-Chain Magnets Exhibiting Quantum Tunneling of Magnetization

Nicole E. Chakov,[†] Wolfgang Wernsdorfer,[‡] Khalil A. Abboud,[†] and George Christou*[,†]

Department of Chemistry, University of Florida, Gainesville, Florida 32611-7200, and Laboratoire Louis Néel-CNRS, BP 166, 25 Avenue des Martyrs, 38042 Grenoble, Cedex 9, France

Received May 6, 2004

The syntheses, structures, and magnetic properties of two new Mn_7 complexes containing phenylseleninate ligands are reported. $[Mn_7O_8(O_2SePh)_8(O_2CMe)(H_2O)]$ (**1**) and $[Mn_7O_8(O_2SePh)_9(H_2O)]$ (**2**) were both prepared by the reaction of 18 equiv of benzeneseleninic acid ($PhSeO_2H$) with $[Mn_{12}O_{12}(O_2CMe)_{16}(H_2O)_4]$ in MeCN. Complex **1**·6MeCN crystallizes in the triclinic space group $P\bar{1}$, and complex **2**·$2CH_2Cl_2$ crystallizes in the monoclinic space group $P2_1/m$. Both compounds possess an unprecedented $[Mn_7O_8]^{9+}$ core comprising a central $[Mn^{III}_3(\mu_3\text{-}O)_4]^{+}$ unit attached to $[Mn^{IV}_2(\mu\text{-}O)_2]^{4+}$ and $[Mn^{IV}_2(\mu\text{-}O)(\mu_3\text{-}O)]^{4+}$ units on either side. In each cluster, the $PhSeO_2^-$ groups function as bridging ligands between adjacent Mn centers. The structure reveals strong Se···O intermolecular contacts between Mn_7 units to give a one-dimensional chain structure, with weak interchain interactions. Solid-state DC magnetic susceptibility measurements of complexes **1** and **2** reveal that they have very similar properties, and detailed studies on **1** by AC susceptibility measurements confirm an $S = 2$ ground-state spin value. In addition, out-of-phase AC signals are observed, suggesting slow magnetization relaxation. Magnetization versus DC field sweeps down to 0.04 K reveals hysteresis loops, but the temperature dependence of the coercivity is not what is expected of a single-molecule magnet. Instead, the behavior is due to single-chain magnetism, albeit with weak antiferromagnetic interactions between the chains, with the barrier to relaxation arising from a combination of molecular anisotropy and ferromagnetic intermolecular exchange interactions mediated by the Se···O contacts. An Arrhenius plot was constructed from the magnetization versus time decay data. The thermally activated region at >0.5 K gave an effective relaxation barrier (U_{eff}) of 14.2 K. Below ~0.1 K, the relaxation is independent of temperature, which is characteristic of magnetization quantum tunneling through the anisotropy barrier. These Mn_7 compounds are thus the first single-chain magnets to comprise polynuclear metal clusters and also the first for which the temperature-independent relaxation characteristic of tunneling has been identified. The work also emphasizes that out-of-phase AC signals for ostensibly molecular compounds are not sufficient proof by themselves of a single-molecule magnet.

Introduction

There are many motivations for the preparation of new polynuclear Mn clusters, not least of which is the structural beauty that such complexes often display. However, a more practical and major objective is the search for new examples of molecules with significant values of ground-state spin, *S*. Indeed, Mn chemistry has proven to be a fertile source of such species. In cases where *S* is fairly large and there is also a significant magnetoanisotropy of the easy-axis (or Ising) type, as reflected in a negative value of the zero-field splitting (ZFS) parameter *D*, such molecules will have a significant energy barrier to relaxation of the magnetization vector and will thus function as single-molecule magnets (SMMs). The upper limit of the energy barrier is given by $S^2|D|$ or $(S^2 - {}^1/_4)|D|$ for integer and half-integer *S* values, respectively. Experimental evidence for SMMs is provided by the observation of frequency-dependent, out-of-phase AC susceptibility signals (χ_M'') and by the hysteresis loops in

* Author to whom correspondence should be addressed. E-mail: christou@chem.ufl.edu.
[†] University of Florida.
[‡] Laboratoire Louis Néel-CNRS.

10.1021/ic0494049 CCC: $27.50
Published on Web 08/24/2004

magnetization versus DC field scans; both properties are characteristic of a superparamagnet-like particle.[1] Additionally, several SMMs display steplike features in the hysteresis loops, a consequence of quantum tunneling of the magnetization (QTM).[2]

The two preparative strategies that have typically been employed previously for preparing new SMMs (and new Mn_x clusters in general) are the following: (i) ligand substitution of some or all of the peripheral ligands in preformed compounds with retention of the core structure[3,4] and (ii) structural transformation of a given Mn_x core to a new structural type by reaction with some suitably chosen chelate or other reagent.[5] Of the SMMs known to date, the $[Mn_{12}O_{12}(O_2CR)_{16}(H_2O)_4]$ family is the most thoroughly studied, exhibiting SMM behavior at the highest temperatures.[1−4,6] A number of Mn_{12} derivatives have been prepared through the use of ligand-substitution reactions on the parent Mn_{12} complex (R = Me), allowing the solubility and redox properties of the clusters to be tuned.[3,4] Mn_{12} compounds are also good starting materials for preparing other high-nuclearity Mn complexes. They have been used in this capacity for preparing a number of high-nuclearity products, and some of these have also proven to be new additions to the SMM family, including the largest Mn−carboxylate cluster obtained to date, $[Mn_{84}O_{72}(O_2CMe)_{78}(OMe)_{24}(MeOH)_{12}(H_2O)_{42}(OH)_6]$.[7]

As part of this general characterization of the reactivity properties of Mn_{12} complexes, we have recently been studying the replacement of some or all of the carboxylate ligands with non-carboxylate ones. This has included the replacement of the carboxylate ligands in a site-specific manner, enhancing reactivity at selected sites and making site-specific reactions feasible. Published progress along these lines includes the site-selective replacement of some of the carboxylate groups with nitrate, diphenylphosphinate, and benzenesulfonate anions (by reactions of $[Mn_{12}O_{12}(O_2CMe)_{16}(H_2O)_4]$ with the corresponding conjugate acids) to give $[Mn_{12}O_{12}(O_2CCH_2Bu^t)_{12}(NO_3)_4(H_2O)_4]$,[8] $[Mn_{12}O_{12}(O_2CMe)_8(O_2PPh_2)_8(H_2O)_4]$,[9] and $[Mn_{12}O_{12}(O_2CMe)_8(O_3SPh)_8(H_2O)_4]$,[10] respectively. In addition, other groups have reported the replacement of four carboxylate groups with diphenylphosphates to give $[Mn_{12}O_{12}(O_2CPh)_{12}(O_2P(OPh)_2)_4(H_2O)_4]$.[11] In all of these cases, the $[Mn_{12}O_{12}]^{16+}$ core is retained intact, although occasionally slightly distorted compared with that of the all-carboxylate parent compound.

The present report is an extension of these studies in a new direction: the reaction of $[Mn_{12}O_{12}(O_2CMe)_{16}(H_2O)_4]$ with benzeneseleninic acid ($PhSeO_2H$). The latter is significantly different from both $Ph_2PO_2^-$ and $PhSO_3^-$, containing only a three-coordinate central atom; however, it is also unlike carboxylate and nitrate groups in that the Se possesses a stereoactive lone pair. In fact, we have found that the $PhSeO_2H$ causes the rupture of the $[Mn_{12}O_{12}]$ core and gives products of an unprecedented structural type containing a $[Mn^{III}_3Mn^{IV}_4O_8]^{9+}$ core. Herein, we report the syntheses, single-crystal X-ray structures, and magnetic properties of two related examples of this new Mn_7 complex.

Experimental Section

Syntheses. All manipulations were performed under aerobic conditions using materials as they were received, except where otherwise noted. $[Mn_{12}O_{12}(O_2CMe)_{16}(H_2O)_4]\cdot 4H_2O\cdot 2MeCO_2H$ (**3**) was prepared as described elsewhere.[12]

$[Mn_7O_8(O_2CMe)(O_2SePh)_8(H_2O)]$ (1). To a stirred solution of complex **3** (0.50 g, 0.24 mmol) in MeCN (75 cm^3) was added solid $PhSeO_2H$ (0.83 g, 4.4 mmol) in portions, and the mixture was stirred for 12 h. The deep-brown solution containing some brown powder was filtered through Celite. The volume of the filtrate was reduced by half by rotoevaporation, and it was then allowed to evaporate slowly in air. Crystals formed slowly over 1 week, and these were suitable for X-ray studies if maintained in contact with the mother liquor to prevent the loss of interstitial solvent. After 1 week, the crystals were isolated by filtration, washed with small volumes of MeCN, and dried under vacuum (yield ∼35%). The dried crystals are hygroscopic, and analyze for $\mathbf{1}\cdot 2H_2O\cdot {}^1/_2MeCN$. Anal. Calcd (found) for $C_{51}H_{50.5}Se_8N_{0.5}O_{29}Mn_7$: C, 28.25 (28.26); H, 2.44 (2.37); N, 0.32 (0.29). Selected IR data (KBr, cm^{-1}): 1636 (w), 1542 (m), 1474 (m), 1441 (m), 1419 (m), 1172 (w), 1094 (m), 1063 (m), 1021 (w), 997 (w), 747 (vs), 712 (vs), 686 (vs), 623 (s), 599 (s), 528 (s), 439 (m).

$[Mn_7O_8(O_2SePh)_9(H_2O)]$ (2). A solution of complex **3** (0.50 g, 0.24 mmol) in MeCN (75 cm^3) was treated with solid $PhSeO_2H$ (0.83 g, 4.4 mmol) in portions. The reaction mixture was stirred for 48 h, during which time the amount of a brown precipitate continuously increased. The latter was collected by filtration, redissolved in CH_2Cl_2 (30 cm^3), and filtered through Celite. Vapor diffusion of Et_2O into the CH_2Cl_2 solution slowly produced crystals, and these were suitable for X-ray crystallography if maintained in contact with the mother liquor to prevent the loss of interstitial solvent. After 2 weeks, crystals were isolated by filtration, washed with Et_2O, and dried under vacuum (yield 40%). The dried material is hygroscopic, analyzing for $\mathbf{2}\cdot 2H_2O$. Anal. Calcd (found) for

(1) (a) Caneschi, A.; Gatteschi, D.; Sessoli, R. *J. Am. Chem. Soc.* **1991**, *113*, 5873. (b) Sessoli, R.; Gatteschi, D.; Caneschi, A.; Novak, M. A. *Nature* **1993**, *365*, 141.

(2) (a) Friedman, J. R.; Sarachik, M. P. *Phys. Rev. Lett.* **1996**, *76*, 3830. (b) Thomas, L.; Lionti, F.; Ballou, R.; Gatteschi, D.; Sessoli, R.; Barbara, B. *Nature* **1996**, *383*, 145. (c) Tejada, J.; Ziolo, R. F.; Zhang, X. X. *Chem. Mater.* **1996**, *8*, 1784.

(3) (a) Eppley, H. J.; Tsai, H.-L.; de Vries, N.; Folting, K.; Christou, G.; Hendrickson, D. N. *J. Am. Chem. Soc.* **1995**, *117*, 301. (b) Eppley, H. J.; Christou, G.; Law, N. A.; Pecoraro, V. L. *Inorg. Synth.* **2002**, *33*, 61.

(4) Soler, M.; Artus, P.; Folting, K.; Huffman, J. C.; Hendrickson, D. N.; Christou, G. *Inorg. Chem.* **2001**, *40*, 4902.

(5) Aromí, G.; Aubin, S. M. J.; Bolcar, M. A.; Christou, G.; Eppley, H. J.; Folting, K.; Hendrickson, D. N.; Huffman, J. C.; Squire, R. C.; Tsai, H.-L.; Wang, S.; Wemple, M. W. *Polyhedron* **1998**, *17*, 3005 and references cited therein.

(6) (a) Christou, G.; Gatteschi, D.; Hendrickson, D. N.; Sessoli, R. *MRS Bull.* **2000**, *25*, 66. (b) Sessoli, R.; Tsai, H.-L.; Schake, A. R.; Wang, S.; Vincent, J. B.; Folting, K.; Gatteschi, D.; Christou, G.; Hendrickson, D. N. *J. Am. Chem. Soc.* **1993**, *115*, 1804. (c) Sessoli, R.; Gatteschi, D.; Caneschi, A.; Novak, M. A. *Nature* **1993**, *365*, 141.

(7) Tasiopoulos, A. J.; Vinslava, A.; Wernsdorfer, W.; Abboud, K. A.; Christou, G. *Angew. Chem., Int. Ed.* **2004**, *43*, 2117.

(8) Artus, P.; Boskovic, C.; Yoo, J.; Streib, W. E.; Brunel, L.-C.; Hendrickson, D. N.; Christou, G. *Inorg. Chem.* **2001**, *40*, 4199.

(9) Boskovic, C.; Pink, M.; Huffman, J. C.; Hendrickson, D. N.; Christou, G. *J. Am. Chem. Soc.* **2001**, *123*, 9914.

(10) Chakov, N. E.; Wernsdorfer, W.; Abboud, K. A.; Hendrickson, D. N.; Christou, G. *J. Chem. Soc., Dalton Trans.* **2003**, *11*, 2243.

(11) Kuroda-Sowa, T.; Fukuda, S.; Miyoshi, S.; Maekawa, M.; Munakata, M.; Miyasaka, H.; Yamashita, M. *Chem. Lett.* **2002**, *31*, 682.

(12) Lis, T. *Acta Crystallogr.* **1980**, *B36*, 2042.

$C_{54}H_{51}Se_9O_{29}Mn_7$: C, 28.71 (28.65); H, 2.28 (2.19); N, 0.00 (0.02). Selected IR data (KBr, cm^{-1}): 3054 (w), 1650 (w), 1635 (w), 1576 (w), 1540 (w), 1475 (w), 1441 (m), 1418 (w), 1336 (w), 1176 (w), 1065 (m), 1021 (w), 998 (w), 744 (vs), 709 (vs), 687 (vs), 622 (s), 599 (s), 530 (s).

X-ray Crystallography. Data were collected using a Siemens SMART PLATFORM equipped with a CCD area detector and a graphite monochromator utilizing Mo Kα radiation ($\lambda = 0.71073$ Å). Suitable single crystals of **1**·6MeCN and **2**·$2CH_2Cl_2$ were separately attached to a glass fiber using silicone grease and transferred to the goniostat where they were cooled to −100 °C for characterization and data collection. Each structure was solved by direct methods (SHELXTL) and standard Fourier techniques and was refined using full-matrix least-squares methods. All non-hydrogen atoms were refined anisotropically. Hydrogen atoms were placed in calculated positions and refined with the use of a riding model. Cell parameters were refined using up to 8192 reflections. For each complex, a full sphere of data (1850 frames) was collected using the ω-scan method (0.3° frame width). The first 50 frames were remeasured at the end of data collection to monitor instrument and crystal stability (maximum correction on I was <1%). Absorption corrections by integration were applied based on measured indexed crystal faces.

A preliminary search of reciprocal space for **1**·6MeCN revealed a set of reflections with no symmetry and no systematic absences. An initial choice of the centrosymmetric space group $P\bar{1}$ was subsequently confirmed by the successful solution of the structure. The asymmetric unit contains the Mn_7 molecule and six disordered MeCN molecules. The solvent molecules could not be modeled properly, and the SQUEEZE program, a part of the PLATON package of crystallographic software, was used to calculate the solvent disorder area and remove its contribution to the overall intensity data. The phenyl rings in two of the $PhSeO_2^-$ ligands [C(7)−C(12) and C(43)−C(48)] were disordered. Their site occupancy factors were dependently refined to 85:15 and 70:30, respectively. Atoms of the minor disorder position in each case were refined with isotropic thermal parameters. Both Se(4) and Se(5) were disordered about two (main) positions and the occupancies refined to 76:24 and 51:49, respectively; the phenyl rings in these ligands were not involved in the disorder. Additionally, the acetate ligand bridging Mn(4)−Mn(5) was disordered about two positions, where the minor disorder position was bridging Mn(3)−Mn(4). This disorder was very minor and could not be modeled; a peak of 1.68 e $Å^{-3}$ appears where the acetate central atom [C(49)] should be, but the corresponding methyl peak [C(50)] could not be found and properly refined. A total of 830 parameters were refined in the final cycle of refinement using 33 358 reflections with $I > 2\sigma(I)$ to yield R1 and wR2 of 5.91 and 14.96%, respectively. The final difference Fourier map was essentially featureless, with the largest peak being 1.68 e $Å^{-3}$ and the deepest hole being −0.78 e $Å^{-3}$.

For complex **2**·$2CH_2Cl_2$, an initial survey of a portion of reciprocal space located a set of reflections with a monoclinic lattice. Analysis of the full data set revealed that the space group was $P2_1/m$. The asymmetric unit contains half of the Mn_7 molecule and one disordered CH_2Cl_2 molecule. The solvent molecule was disordered and could not be modeled properly, so the SQUEEZE program was used to calculate the solvent disorder area and remove its contribution to the overall intensity data. The phenyl rings in two of the $PhSeO_2^-$ ligands [C(1)−C(6) and C(51)−C(56)] were disordered about the crystallographic mirror plane that bisects the molecule. Their site occupancy factors were fixed at 50%. Additionally, the phenyl rings in two $PhSeO_2^-$ ligands not centered over the mirror plane [C(31)−C(36) and C(41)−C(46)] were disordered over two sites. Their site occupancy factors were dependently refined to 53:47 and 50:50, respectively; atoms of minor disorder positions were refined with isotropic thermal parameters. Se(2) and its phenyl ring were disordered about two positions and the occupancies dependently refined to 67:33 and 32:68, respectively. Finally, Se(6) and its phenyl ring [C(61)−C(66)] bridge Mn(2)−Mn(4) and, because of the mirror symmetry, Mn(4)−Mn(2A). The disorder is with a water molecule. The site occupancy factors were refined to 50%. As a precaution, the structure was also solved and refined in space group $P2_1$, with the mirror symmetry removed, but the amount of disorder was not changed compared with that of the structure in space group $P2_1/m$. A total of 328 parameters were refined in the final cycle of refinement using 29 004 reflections with $I > 2\sigma(I)$ to yield R1 and wR2 of 8.73 and 24.55%, respectively. The final difference Fourier map was essentially featureless, with the largest peak and deepest hole being at 1.704 and −1.540 e $Å^{-3}$, respectively.

Table 1. Crystallographic Data for Complexes **1**·6MeCN and **2**·$2CH_2Cl_2$

	1	**2**
formula[a]	$C_{62}H_{63}Se_8Mn_7N_6O_{27}$	$C_{56}H_{51}Cl_4Se_9Mn_7O_{27}$
fw (g mol^{-1})	2340.45	2393.02
space group	$P\bar{1}$	$P2_1/m$
a (Å)	10.7432(8)	10.7776(7)
b (Å)	15.1584(11)	27.7484(8)
c (Å)	24.3955(18)	13.4463(9)
α (deg)	99.639(2)	90
β (deg)	91.197(2)	105.670(2)
γ (deg)	105.776(2)	90
V ($Å^3$)	3759.9(5)	3871.8(4)
Z	2	2
T (°C)	−100(2)	−100(2)
radiation (Å)[b]	0.71073	0.71073
ρ_{calc} (g cm^{-3})	2.067	2.053
μ (cm^{-1})	50.94	55.48
R1 (wR2) (%)[c,d]	5.91 (14.96)	8.73 (24.55)

[a] Including solvent molecules. [b] Graphite monochromator. [c] $R1 = \sum||F_o| - |F_c||/\sum|F_o|$. [d] $wR2 = [\sum[w(F_o^2 - F_c^2)^2]/\sum[w(F_o^2)^2]]^{1/2}$, where $S = [\sum[w(F_o^2 - F_c^2)^2]/(n - p)]^{1/2}$, $w = 1/[\sigma^2(F_o^2) + (mp)^2 + np]$, $p = [\max(F_o^2,0) + 2F_c^2]/3$, and m and n are constants.

The crystallographic data and structure refinement details are collected in Table 1.

Other Studies. Infrared spectra were recorded in the solid state (KBr pellets) on a Nicolet Nexus 670 FTIR spectrophotometer in the 400−4000 cm^{-1} range. Elemental analyses (C, H, and N) were performed at the in-house facilities of the University of Florida's Chemistry Department. Variable temperature DC magnetic susceptibility data down to 1.80 K were collected on a Quantum Design MPMS-XL SQUID magnetometer equipped with a 70 kG (7 T) DC magnet at the University of Florida. Pascal's constants were used to estimate the diamagnetic corrections, which were subtracted from the experimental susceptibility to give the molar magnetic susceptibility (χ_M). AC magnetic susceptibility data were collected on the same instrument employing a 3.5 G field oscillating at frequencies up to 1500 Hz. DC measurements below 1.80 K were performed on single crystals using an array of micro-SQUIDS.[13]

Results and Discussion

Syntheses. Our initial attempts to introduce $PhSeO_2^-$ groups into high-nuclearity Mn aggregates involved the reactions of benzeneseleninic acid with several trinuclear and tetranuclear complexes containing the [$Mn_3(\mu_3$-O)] and [Mn_4-

(13) Wernsdorfer, W. *Adv. Chem. Phys.* **2001**, *118*, 99.

(μ_3-O)$_2$] cores, respectively. These were known from previous work to yield magnetically interesting complexes upon reaction with a chelating ligand.[14,15] However, despite many attempts, such reactions were ineffective, and spectroscopic characterization of the products indicated that no reaction between the Mn complexes and $PhSeO_2H$ had occurred. This is likely due to a combination of effects, including the poor solubility of the ligand in the MeCN solvent and the essentially identical acid dissociation constants of $PhSeO_2H$ ($pK_a = 4.79$) and $MeCO_2H$ ($pK_a = 4.76$);[16] a large difference in pK_a values facilitates the substitution of $MeCO_2^-$ ligands.

We thus turned our attention to the reactions of the acid with $[Mn_{12}O_{12}(O_2CMe)_{16}(H_2O)_4]$, thinking that this might allow at least some $PhSeO_2^-$ groups to be incorporated around the $[Mn_{12}O_{12}]$ core, as had been found with $PhSO_3^-$. Thus, complex **3** in distilled MeCN was treated with 18 equiv of $PhSeO_2H$, which slowly dissolved. After 12 h, the resulting deep-brown solution was separated by filtration from some brown powder, and from the filtrate was obtained a dark-brown crystalline product. It was immediately obvious from the infrared spectrum that the reaction had led to the transformation of the $[Mn_{12}O_{12}]$ core of **3**, and the product was subsequently identified by X-ray crystallography as $[Mn_7O_8(O_2CMe)(O_2SePh)_8(H_2O)]$ (**1**), obtained in ~35% yield.

When the same reaction system was maintained for longer reaction times, the amount of the brown precipitate steadily increased. After 48 h, the precipitate was collected by filtration and recrystallized from CH_2Cl_2/Et_2O to give crystals of $[Mn_7O_8(O_2SePh)_9(H_2O)]$ (**2**) in 40% yield. The overall transformations to give **1** and **2** are summarized in eq 1, which has been formulated for product **1**; that for **2** would be very similar.

$$[Mn_{12}O_{12}(O_2CMe)_{16}(H_2O)_4] + 8PhSeO_2H \rightarrow [Mn_7O_8(O_2CMe)(O_2SePh)_8(H_2O)] + 7H_2O + 5Mn^{3+} + 15MeCO_2^- \quad (1)$$

Charge considerations and the inspection of metric parameters indicate that **1** and **2** are mixed-valence $3Mn^{III}$ and $4Mn^{IV}$, with a trapped-valence situation (vide infra). Clearly, the overall conversion of $[Mn_{12}O_{12}(O_2CMe)_{16}(H_2O)_4]$ ($8Mn^{III}$, $4Mn^{IV}$) into these products must involve a complicated mechanism involving fragmentation and recombination steps. There are almost certainly other species left in the colored filtrates after the product crystals are collected (these are likely Mn^{III} acetate species), but we have not explored these further. Since complexes **1** and **2** are so similar, differing only in the identity of one ligand (acetate vs benzeneselenate), we were fortunate that they have significantly different solubilities in MeCN because their isolation in pure form would not otherwise have been possible. Complex **1** is fairly soluble in MeCN, whereas **2** is not. Thus, at shorter reaction times, we were able to obtain **1** from the filtered reaction solution, whereas at longer reaction times, substitution of its remaining acetate by another $PhSeO_2^-$ group converts it to **2**, which precipitates from the solution.

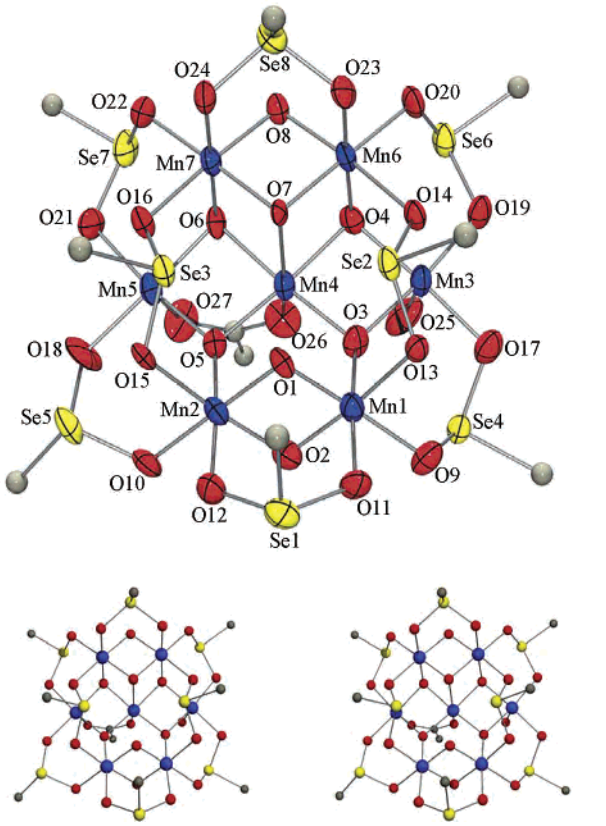

Figure 1. ORTEP representation in PovRay format of complex **1** at the 50% probability level, together with a stereopair. For clarity, the hydrogen atoms have been omitted and only the *ipso* C atoms of the phenyl groups are shown.

X-ray Crystal Structure of Complex 1. A labeled ORTEP plot in PovRay format of complex **1** is shown in Figure 1, together with a stereoview. Selected interatomic distances and angles are listed in Table 2. The complex crystallizes in the triclinic space group $P\bar{1}$, with the Mn_7 molecule in a general position. The structure consists of a $[Mn^{III}_3Mn^{IV}_4(\mu_3\text{-}O)_5(\mu\text{-}O)_3]^{9+}$ core (Figure 2a), with the peripheral ligation provided by eight bridging $PhSeO_2^-$ ligands, one bridging $MeCO_2^-$ ligand, and one terminal H_2O molecule. Bond valence sum (BVS) calculations[17] indicate a mixed-valence, trapped-valence complex; Mn(3), Mn(4), and Mn(5) are Mn^{III}, while the remaining Mn centers Mn(1), Mn(2), Mn(6), and Mn(7) are Mn^{IV}. Each Mn^{IV} ion is in a distorted octahedral environment. The two outer Mn^{III} ions, Mn(3) and Mn(5), are five-coordinate with a square pyramidal geometry ($\tau = 0.06$ and 0.07, respectively, where τ is 0 and 1 for ideal square pyramidal and trigonal

(14) (a) Vincent, J. B.; Christmas, C.; Chang, H.-R.; Li, Q.; Boyd, P. D. W.; Huffman, J. C.; Hendrickson, D. N.; Christou, G. *J. Am. Chem. Soc.* **1989**, *111*, 2086. (b) Libby, E.; McCusker, J. K.; Schmitt, E. A.; Folting, K.; Hendrickson, D. N.; Christou, G. *Inorg. Chem.* **1991**, *30*, 3486. (c) Bouwman, E.; Bolcar, M. A.; Libby, E.; Huffman, J. C.; Folting, K.; Christou, G. *Inorg. Chem.* **1992**, *31*, 5185. (d) Wang, S.; Huffman, J. C.; Folting, K.; Streib, W. E.; Lobkovsky, E. B.; Christou, G. *Angew. Chem., Int. Ed. Engl.* **1991**, *30*, 1672.

(15) Brechin, E. K.; Boskovic, C.; Wernsdorfer, W.; Yoo, J.; Yamaguchi, A.; Sañudo, E. C.; Concolino, T. R.; Rheingold, A. L.; Ishimoto, H.; Hendrickson, D. N.; Christou, G. *J. Am. Chem. Soc.* **2002**, *124*, 9710.

(16) McCullough, J.; Gould, E. S. *J. Am. Chem. Soc.* **1949**, *71*, 674.

(17) Palenik, G. J. *Inorg. Chem.* **1997**, *36*, 4888.

Table 2. Bond Distances (Å) and Angles (deg) for Complex **1**

Mn(1)−O(1)	1.788(6)	Mn(3)−O(19)	1.923(6)	Mn(5)−O(21)	1.950(6)
Mn(1)−O(2)	1.839(7)	Mn(3)−O(25)	2.289(8)	Mn(5)−O(27)	2.172(8)
Mn(1)−O(3)	1.914(6)	Mn(3)−Mn(4)	2.856(2)	Mn(5)−Mn(7)	3.126(2)
Mn(1)−O(11)	1.944(6)	Mn(3)−Mn(3)	3.111(2)	Mn(6)−O(8)	1.831(6)
Mn(1)−O(9)	1.961(6)	Mn(4)−O(5)	1.895(6)	Mn(6)−O(7)	1.848(6)
Mn(1)−O(13)	1.998(6)	Mn(4)−O(3)	1.907(6)	Mn(6)−O(4)	1.899(7)
Mn(1)−Mn(2)	2.722(2)	Mn(4)−O(4)	1.944(6)	Mn(6)−O(23)	1.909(7)
Mn(2)−O(1)	1.813(6)	Mn(4)−O(6)	1.949(6)	Mn(6)−O(14)	1.994(6)
Mn(2)−O(2)	1.844(7)	Mn(4)−O(26)	2.180(7)	Mn(6)−Mn(7)	2.758(2)
Mn(2)−O(5)	1.905(6)	Mn(4)−O(7)	2.278(6)	Mn(7)−O(8)	1.819(6)
Mn(2)−O(12)	1.948(6)	Mn(4)−Mn(5)	2.829(2)	Mn(7)−O(7)	1.852(5)
Mn(2)−O(10)	1.992(7)	Mn(4)−Mn(6)	3.018(2)	Mn(7)−O(6)	1.886(6)
Mn(2)−O(15)	2.002(6)	Mn(4)−Mn(7)	3.036(2)	Mn(7)−O(24)	1.935(7)
Mn(3)−O(3)	1.893(6)	Mn(5)−O(5)	1.880(6)	Mn(7)−O(16)	1.960(6)
Mn(3)−O(4)	1.898(6)	Mn(5)−O(6)	1.907(6)	Mn(7)−O(22)	1.964(6)
Mn(3)−O(17)	1.918(6)	Mn(5)−O(18)	1.909(7)		
O(1)−Mn(1)−O(2)	83.7(3)	O(4)−Mn(3)−O(25)	89.4(3)	O(4)−Mn(4)−O(7)	75.4(2)
O(1)−Mn(1)−O(3)	93.3(3)	O(17)−Mn(3)−O(25)	89.3(3)	O(6)−Mn(4)−O(7)	74.4(2)
O(2)−Mn(1)−O(3)	90.0(3)	O(19)−Mn(3)−O(25)	94.0(3)	O(26)−Mn(4)−O(7)	160.8(2)
O(1)−Mn(1)−O(11)	92.8(3)	O(5)−Mn(4)−O(3)	100.4(3)	O(5)−Mn(5)−O(6)	83.8(3)
O(2)−Mn(1)−O(11)	90.0(3)	O(7)−Mn(6)−O(20)	175.5(3)	O(5)−Mn(5)−O(18)	96.2(3)
O(1)−Mn(1)−O(13)	89.4(3)	O(4)−Mn(6)−O(20)	88.3(3)	O(6)−Mn(5)−O(18)	176.2(4)
O(2)−Mn(1)−O(13)	173.0(3)	O(23)−Mn(6)−O(20)	92.1(3)	O(5)−Mn(5)−O(21)	172.1(3)
O(3)−Mn(1)−O(13)	91.5(3)	O(8)−Mn(6)−O(14)	172.1(3)	O(6)−Mn(5)−O(21)	90.2(3)
O(11)−Mn(1)−O(13)	89.3(3)	O(7)−Mn(6)−O(14)	90.2(2)	O(18)−Mn(5)−O(21)	89.3(3)
O(9)−Mn(1)−O(13)	89.8(3)	O(4)−Mn(6)−O(14)	87.2(3)	O(5)−Mn(5)−O(27)	90.1(3)
O(1)−Mn(2)−O(2)	82.8(3)	O(23)−Mn(6)−O(14)	89.4(3)	O(6)−Mn(5)−O(27)	89.4(3)
O(1)−Mn(2)−O(5)	92.3(3)	O(20)−Mn(6)−O(14)	91.6(2)	O(18)−Mn(5)−O(27)	94.5(4)
O(2)−Mn(2)−O(5)	91.3(3)	O(8)−Mn(7)−O(7)	82.8(2)	O(21)−Mn(5)−O(27)	95.1(3)
O(1)−Mn(2)−O(12)	92.7(3)	O(8)−Mn(7)−O(6)	93.5(3)	O(8)−Mn(6)−O(7)	82.6(2)
O(2)−Mn(2)−O(12)	89.8(3)	O(7)−Mn(7)−O(6)	86.8(3)	O(8)−Mn(6)−O(4)	95.8(3)
O(5)−Mn(2)−O(12)	174.9(3)	O(8)−Mn(7)−O(24)	88.4(3)	O(7)−Mn(6)−O(4)	87.6(3)
O(1)−Mn(2)−O(10)	179.0(3)	O(3)−Mn(1)−O(11)	173.9(3)	O(8)−Mn(6)−O(23)	87.5(3)
O(2)−Mn(2)−O(10)	97.0(3)	O(1)−Mn(1)−O(9)	176.4(3)	O(7)−Mn(6)−O(23)	92.1(3)
O(5)−Mn(2)−O(10)	88.7(3)	O(2)−Mn(1)−O(9)	97.0(3)	O(4)−Mn(6)−O(23)	176.6(3)
O(12)−Mn(2)−O(10)	86.3(3)	O(3)−Mn(1)−O(9)	90.3(3)	O(8)−Mn(6)−O(20)	95.8(3)
O(1)−Mn(2)−O(15)	90.9(3)	O(11)−Mn(1)−O(9)	83.6(3)	O(7)−Mn(7)−O(24)	91.7(3)
O(2)−Mn(2)−O(15)	173.7(3)	O(5)−Mn(4)−O(4)	173.6(3)	O(6)−Mn(7)−O(24)	177.4(3)
O(5)−Mn(2)−O(15)	89.8(3)	O(3)−Mn(4)−O(4)	81.9(3)	O(8)−Mn(7)−O(16)	174.4(3)
O(12)−Mn(2)−O(15)	89.7(3)	O(5)−Mn(4)−O(6)	82.3(3)	O(7)−Mn(7)−O(16)	91.9(3)
O(10)−Mn(2)−O(15)	89.2(3)	O(3)−Mn(4)−O(6)	174.0(3)	O(6)−Mn(7)−O(16)	88.2(3)
O(3)−Mn(3)−O(4)	83.5(3)	O(4)−Mn(4)−O(6)	94.9(3)	O(24)−Mn(7)−O(16)	89.7(3)
O(3)−Mn(3)−O(17)	93.9(3)	O(5)−Mn(4)−O(26)	90.9(3)	O(8)−Mn(7)−O(22)	96.4(3)
O(4)−Mn(3)−O(17)	177.1(3)	O(3)−Mn(4)−O(26)	95.0(3)	O(7)−Mn(7)−O(22)	175.5(3)
O(3)−Mn(3)−O(19)	173.5(3)	O(4)−Mn(4)−O(26)	94.9(3)	O(6)−Mn(7)−O(22)	88.8(3)
O(4)−Mn(3)−O(19)	90.7(3)	O(6)−Mn(4)−O(26)	90.3(3)	O(24)−Mn(7)−O(22)	92.8(3)
O(17)−Mn(3)−O(19)	91.9(3)	O(5)−Mn(4)−O(7)	98.3(2)	O(16)−Mn(7)−O(22)	89.0(3)
O(3)−Mn(3)−O(25)	89.0(3)	O(3)−Mn(4)−O(7)	99.8(2)		

bipyramidal geometries, respectively),[18] while the remaining Mn^{III} ion, Mn(4), has a very distorted octahedral geometry.

At first glance, the viewpoints of Figures 1 and 2a suggest that a useful way of describing the core of **1** is as a Mn_6 ring with a seventh Mn in the middle. However, this is not a good description because the Mn_7 unit is far from planar. This is emphasized in the side view of Figure 2b. As can be seen, a much better dissection of the core shows a central $[MnO_2MnO_2Mn]^+$ unit (i.e., $3Mn^{III}$) with its bridging oxide ions on each side attached to a $[MnO_2Mn]^{4+}$ unit ($2Mn^{IV}$). The three Mn^{III} ions in the central unit are ligated on one side by the bridging acetate and terminal water groups (O(25)−O(27)), and these Mn^{III} ions would all be five-coordinate except that one $[MnO_2Mn]^{4+}$ unit swivels about its bridging oxide atoms (O(4) and O(6)) to bring O(7) within bonding distance of Mn(4), making the latter six-coordinate (Mn(4)-O(7) = 2.278 Å). Discrete examples of the $[Mn(\mu\text{-}O)_2Mn]^{4+}$ core in dinuclear complexes are fairly common.[19] But note that only recently, in the $[Mn_8O_{10}(O_2CMe)_6(H_2O)_2(bpy)_6]^{4+}$ cation,[20] has the $[Mn^{IV}{}_2(\mu\text{-}O)(\mu_3\text{-}O)]^{4+}$ variant of these units, as found in **1**, been observed. Note also that the $[MnO_2Mn]^{4+}$ units can alternatively be described as $[MnO_2(O_2SePh)Mn]^{4+}$ units since there is also a $PhSeO_2^-$ bridging them. Thus, they are also very similar to the common dinuclear complexes containing the triply bridged $[Mn_2(\mu\text{-}O)_2(\mu\text{-}O_2CR)]^{2+,3+}$ core.[21,22] In contrast, the central $[MnO_2MnO_2Mn]^+$ fragment, containing a linear Mn_3 unit, has never been seen before in a discrete Mn_3 complex, although it is a commonly encountered subfragment of several higher-nuclearity clusters, such as certain Mn_{10},[23] Mn_{11},[24] and Mn_{18}[15] species. Overall, the complete Mn_7 complex possesses C_1 symmetry.

(18) Jansen, J. C.; Van Koningsveld, H.; Van Ooijen, J. A. C.; Reedijk, J. *Inorg. Chem.* **1980**, *19*, 170.

(19) (a) Law, N. A.; Kampf, J. W.; Pecoraro, V. L. *Inorg. Chim. Acta* **2000**, *297*, 252. (b) Goodson, P. A.; Hodgson, D. J.; Glerup, J.; Michelsen, K.; Weihe, H. *Inorg. Chim. Acta* **1992**, *197*, 141. (c) Goodson, P. A.; Glerup, J.; Hodgson, D. J.; Michelsen, K.; Weihe, H. *Inorg. Chem.* **1991**, *30*, 4909. (d) Larson, E.; Lah, M. S.; Li, X.; Bonadies, J. A.; Pecoraro, V. L. *Inorg. Chem.* **1992**, *31*, 373. (e) Gohdes, J. W.; Armstrong, W. H. *Inorg. Chem.* **1992**, *31*, 368. (f) Libby, E.; Webb, R. J.; Streib, W. E.; Folting, K.; Huffman, J. C.; Hendrickson, D. N.; Christou, G. *Inorg. Chem.* **1989**, *28*, 4037. (g) Pal, S.; Olmstead, M. M.; Armstrong, W. H. *Inorg. Chem.* **1995**, *34*, 4708. (h) Torayama, H.; Asada, H.; Fujiwara, M.; Matsushita, T. *Polyhedron* **1998**, *17*, 3859. (i) Oki, A. R.; Glerup, J.; Hodgson, D. J. *Inorg. Chem.* **1990**, *29*, 2435.

(20) Tasiopoulos, A. J.; Abboud, K. A.; Christou, G. *Chem. Commun.* **2003**, 580.

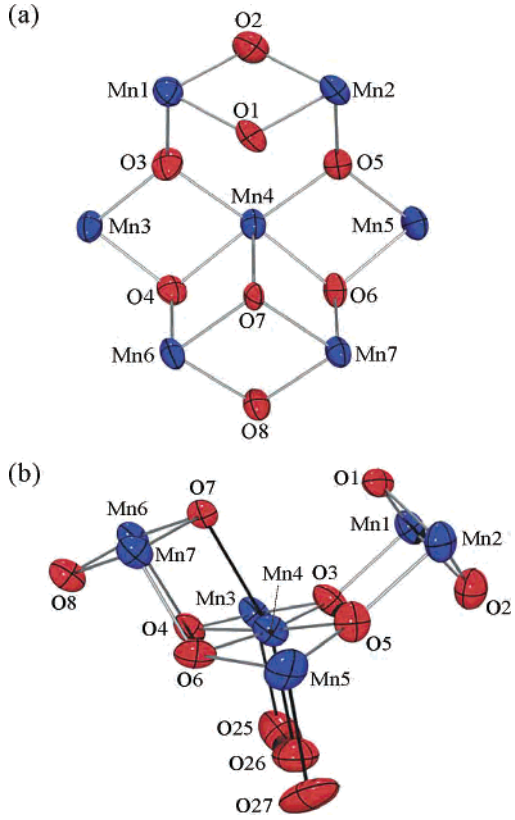

Figure 2. ORTEP representations of (a) the $[Mn_7O_8]^{9+}$ core of complex **1** and (b) the relative disposition of the elongation axes, indicated as black bonds.

The central Mn^{III} ion, Mn(4), displays a Jahn−Teller (JT) axial elongation, as expected for a high-spin Mn^{III} (d^4) ion. Normally, JT elongation axes avoid Mn−oxide bonds, almost always the strongest and shortest in the molecule, but in this case, the oxide O(7) cannot approach too closely and the resulting Mn(4)−O(7) distance (2.278(6) Å) is very long for a Mn−oxide bond, even a JT elongated one. The other JT elongated bond is Mn(4)−O(27) (2.180(7) Å). For the two square pyramidal Mn^{III} ions, Mn(3) and Mn(5), their local *z* axis is oriented parallel to the JT axis of Mn(4). Thus, the long, apical bonds of the sp geometries (Mn(3)−O(25) = 2.289(8) Å and Mn(5)−O(27) = 2.172(8) Å) are parallel to the long bonds at Mn(4). In effect, then, there is parallel alignment of the three Mn^{III} distortion axes, which will dominate the magnetic anisotropy (i.e., the magnitude of the ZFS parameter, *D*) of the complete Mn_7 molecule. This will be of relevance to the magnetic discussion later.

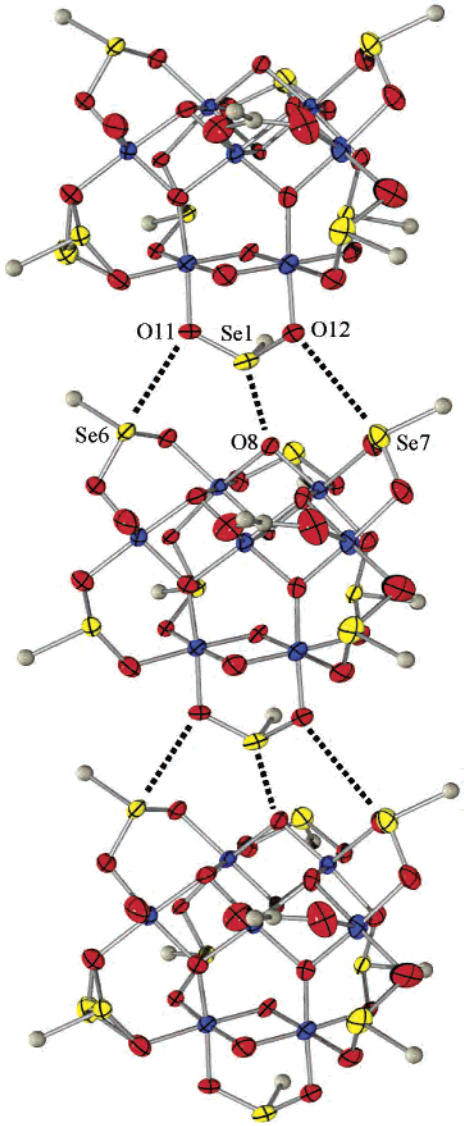

Figure 3. ORTEP representation in PovRay format at the 50% probability level of the packing of complex **1** along the *a* axis of the crystal. For clarity, the hydrogen atoms have been omitted and only the *ipso* C atoms of the phenyl groups are shown.

The Se geometry is pyramidal, due to the presence of a stereochemically active lone pair of electrons. The only previous example of the $PhSeO_2^-$ group bridging in the same manner as seen in **1** was in the polymer $[Ph_3SnO_2SePh]_n$, in which the $PhSeO_2^-$ ligand symmetrically bridges two Sn atoms.[25] There is evidence of strong intermolecular Se···O interactions in **1**, forming chains along the *a* axis of the crystal (Figure 3). The Se(1)···O(8) distance (2.749(6) Å) is longer than the sum of the covalent radii of Se and O

(21) (a) Bashkin, J. S.; Schake, A. R.; Vincent, J. B.; Chang, H.-R.; Li, Q.; Huffman, J. C.; Christou, G.; Hendrickson, D. N. *Chem. Commun.* **1988**, 700. (b) Wieghardt, K.; Bossek, U.; Zsolnai, G.; Huttner, G.; Blondin, G.; Girerd, J.-J.; Babonneau, F. *Chem. Commun.* **1987**, 651. (c) Osawa, M.; Fujisawa, K.; Kitajima, N.; Moro-oka, Y. *Chem. Lett.* **1997**, *26*, 919. (d) Bossek, U.; Saher, M.; Weyhermuller, T.; Wieghardt, K. *Chem. Commun.* **1992**, 1780. (e) Schafer, K.-O.; Bittl, R.; Zweygart, W.; Lendzian, F.; Haselhorst, G.; Weyhermuller, T.; Wieghardt, K.; Lubitz, W. *J. Am. Chem. Soc.* **1998**, *120*, 13104. (f) Lal, T. K.; Mukherjee, R. *Inorg. Chem.* **1998**, *37*, 2373. (g) Pal, S.; Gohdes, J. W.; Wilisch, W. C. A.; Armstrong, W. H. *Inorg. Chem.* **1992**, *31*, 713.

(22) (a) Bhaduri, S.; Tasiopoulos, A. J.; Bolcar, M. A.; Abboud, K. A.; Streib, W. E.; Christou, G. *Inorg. Chem.* **2003**, *42*, 1483. (b) Mok, H. J.; Davis, J. A.; Pal, S.; Mandal, S. K.; Armstrong, W. H. *Inorg. Chim. Acta* **1997**, *263*, 385. (c) Dave, B. C.; Czernuszewicz, R. S.; Bond, M. R.; Carrano, C. J. *Inorg. Chem.* **1993**, *32*, 3593. (d) Reddy, K. R.; Rajasekharan, M. V.; Padhye, S.; Dahan, F.; Tuchagues, J.-P. *Inorg. Chem.* **1994**, *33*, 428. (e) Pal, S.; Chan, M. K.; Armstrong, W. H. *J. Am. Chem. Soc.* **1992**, *114*, 6398. (f) Pal, S.; Armstrong, W. H. *Inorg. Chem.* **1992**, *31*, 5417.

(23) Harden, N. C.; Bolcar, M. A.; Wernsdorfer, W.; Abboud, K. A.; Streib, W. E.; Christou, G. *Inorg. Chem.* **2003**, *42*, 7067.

(24) Perlepes, S. P.; Huffman, J. C.; Christou, G. *Chem. Commun.* **1991**, 1657.

(25) Chandrasekhar, V.; Muralidhara, M. G.; Justin Thomas, K. R.; Tiekink, E. R. T. *Inorg. Chem.* **1992**, *31*, 4707.

Table 3. Bond Distances (Å) and Angles (deg) for Complex **2**

Mn(1)−O(14)	1.800(6)	Mn(2)−O(5)	1.903(10)	Mn(3)−O(9)	1.952(8)
Mn(1)−O(15)	1.845(7)	Mn(2)−O(8)	1.935(8)	Mn(3)−O(7)	2.005(7)
Mn(1)−O(12)	1.886(7)	Mn(2)−O(2)	2.001(17)	Mn(3)−Mn(3A)	2.740(3)
Mn(1)−O(3)	1.932(7)	Mn(2)−Mn(3)	3.114(2)	Mn(3)−Mn(4)	3.034(2)
Mn(1)−O(4)	1.983(8)	Mn(2)−Mn(4)	2.8429(19)	Mn(4)−O(12)	1.913(7)
Mn(1)−O(6)	2.010(8)	Mn(3)−O(11)	1.822(5)	Mn(4)−O(13)	1.963(7)
Mn(1)−Mn(1A)	2.761(3)	Mn(3)−O(16)	1.843(5)	Mn(4)−O(1)	2.160(12)
Mn(2)−O(13)	1.873(8)	Mn(3)−(13)	1.894(8)	Mn(4)−O(16)	2.276(9)
Mn(2)−O(12)	1.902(7)	Mn(3)−O(10)	1.923(7)		
O(14)−Mn(1)−O(15)	81.5(3)	O(16)−Mn(3)−O(9)	176.3(4)	O(8)−Mn(2)−O(2)	89.8(6)
O(14)−Mn(1)−O(12)	92.9(3)	O(13)−Mn(3)−O(9)	89.1(3)	O(11)−Mn(3)−O(16)	83.1(3)
O(15)−Mn(1)−O(12)	90.1(4)	O(10)−Mn(3)−O(9)	91.6(3)	O(11)−Mn(3)−O(13)	94.6(4)
O(14)−Mn(1)−O(3)	93.1(4)	O(11)−Mn(3)−O(7)	173.7(3)	O(16)−Mn(3)−O(13)	87.3(3)
O(15)−Mn(1)−O(3)	89.4(4)	O(16)−Mn(3)−O(7)	90.9(3)	O(11)−Mn(3)−O(10)	89.4(4)
O(12)−Mn(1)−O(3)	173.8(3)	O(13)−Mn(3)−O(7)	86.9(3)	O(16)−Mn(3)−O(10)	92.1(3)
O(14)−Mn(1)−O(4)	177.2(4)	O(10)−Mn(3)−O(7)	89.0(3)	O(12)−Mn(4)−O(12A)	99.9(4)
O(15)−Mn(1)−O(4)	98.8(4)	O(9)−Mn(3)−O(7)	89.8(3)	O(12)−Mn(4)−O(13)	81.8(3)
O(12)−Mn(1)−O(4)	89.9(4)	O(13)−Mn(2)−O(12)	84.5(3)	O(12)−Mn(4)−O(13A)	173.5(3)
O(3)−Mn(1)−O(4)	84.1(4)	O(13)−Mn(2)−O(5)	176.4(4)	O(13)−Mn(4)−O(13A)	95.8(4)
O(14)−Mn(1)−O(6)	90.2(3)	O(12)−Mn(2)−O(5)	92.7(4)	O(12)−Mn(4)−O(1)	94.0(3)
O(15)−Mn(1)−O(6)	171.7(3)	O(13)−Mn(2)−O(8)	88.9(4)	O(13)−Mn(4)−O(1)	92.2(3)
O(12)−Mn(1)−O(6)	91.5(3)	O(12)−Mn(2)−O(8)	171.7(4)	O(12)−Mn(4)−O(16)	98.9(3)
O(3)−Mn(1)−O(6)	89.9(3)	O(5)−Mn(2)−O(8)	94.1(5)	O(13)−Mn(4)−O(16)	74.6(3)
O(4)−Mn(1)−O(6)	89.3(4)	O(13)−Mn(2)−O(2)	92.0(7)	O(1)−Mn(4)−O(16)	160.0(4)
O(13)−Mn(3)−O(10)	175.9(3)	O(12)−Mn(2)−O(2)	95.5(5)		
O(11)−Mn(3)−O(9)	96.3(3)	O(5)−Mn(2)−O(2)	86.1(8)		

(1.89 Å) but much shorter than the sum of their van der Waals radii (3.40 Å). This interaction likely involves an O(p_π) to Se(d_π) donation into empty Se d orbitals. Additionally, the Se(6)−O(11) contact (3.327(6) Å), and perhaps also Se(7)−O(12) (3.643(6) Å), likely contributes to the intermolecular interaction. There is precedent for these types of interactions; there are several examples in the literature of intramolecular Se···O nonbonded interactions, including those in selenoiminoquinones,[26] selenoxocine,[27] and selenazofurin.[28]However, none of these previous examples involves the same kind of seleninate ligands that are present in **1**. There are also numerous weak interchain contacts apparent in the packing diagrams between aromatic rings and/or solvent molecules, but the disorder in these groups discussed in the Experimental Section complicates their clear visualization.

X-ray Crystal Structure of Complex 2. A labeled ORTEP plot in PovRay format of complex **2** is shown in Figure 4, together with a stereoview. Selected interatomic distances and angles are listed in Table 3. The complex crystallizes in the monoclinic space group $P2_1/m$, with the Mn_7 molecule lying on a mirror plane. For the sake of brevity, references to specific atoms in the following discussion implicitly include their symmetry-related partners. The structure of **2** is very similar to that of **1**, except that the $MeCO_2^-$ group in the latter has been replaced with a ninth $PhSeO_2^-$ group. Bond valence sums, again, indicate a $3Mn^{III}$ and $4Mn^{IV}$ trapped-valence situation. The core has the same structure as that for **1** (Figure 2a), with five-coordinate Mn(2) being square pyramidal ($\tau = 0.08$). The $PhSeO_2^-$ for $MeCO_2^-$ substitution causes an almost insignificant perturbation of the core. The long Mn(4)−O(16) bond (2.276(9) Å) is very similar to that in **1**, and the three Mn^{III} distortion axes are again essentially parallel. As

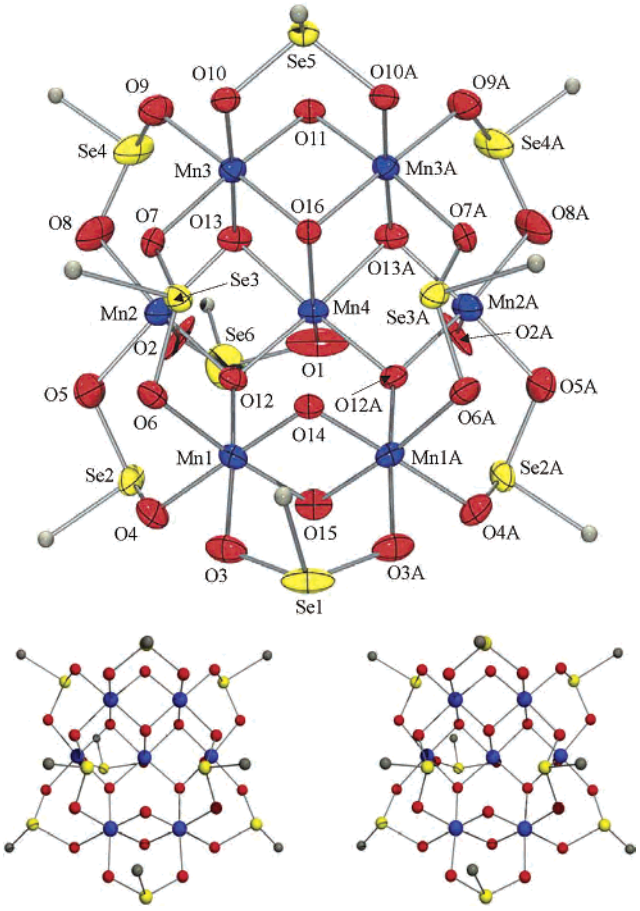

Figure 4. ORTEP representation in PovRay format of complex **2** at the 50% probability level, together with a stereopair. For clarity, the hydrogen atoms have been omitted and only the *ipso* C atoms of the phenyl groups are shown.

(26) Barton, D. H.; Hall, M. B.; Lin, Z.; Parekh, S. I.; Reibenspies, J. *J. Am. Chem. Soc.* **1993**, *115*, 5056.
(27) Fujihara, H.; Nakahodo, T.; Furukawa, N. *Tetrahedron Lett.* **1995**, *36*, 6275.
(28) Goldstein, B. M.; Kennedy, S. D.; Hennen, W. J. *J. Am. Chem. Soc.* **1990**, *112*, 8265.

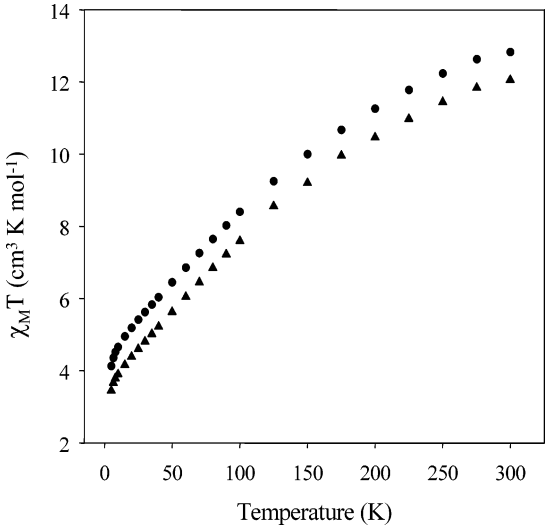

Figure 5. Plot of $\chi_M T$ vs temperature for dried microcrystalline samples of complex **1**·2H_2O·$^1/_2$MeCN (▲) and **2**·2H_2O (●) in eicosane. χ_M is the DC molar magnetic susceptibility measured in a 5.0 kG field.

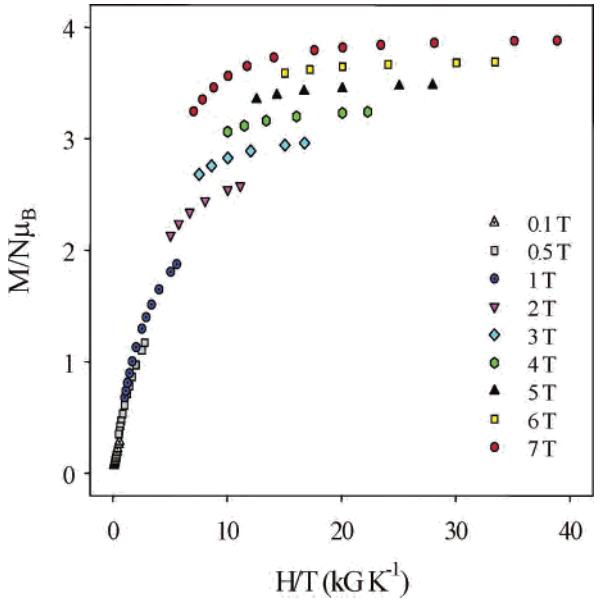

Figure 6. Plot of reduced magnetization ($M/N\mu_B$) vs H/T for a dried microcrystalline sample of **1**·2H_2O·$^1/_2$MeCN; the DC field value of each of the isofield plots is indicated.

observed with complex **1**, there is a strong intermolecular interaction between the Se atoms and the O atoms, forming chains along the *a* axis of the crystal, with weak interchain contacts. The shortest and strongest contact is Se(1)···O(11) (2.754(6) Å).

Complexes **1** and **2** possess a structure that is quite different from those of previously characterized Mn_7 complexes. These include $[Mn^{II}_3Mn^{III}_4(OMe)_{12}(dbm)_6]$ (dbm^- is the anion of dibenzoylmethane),[29] the $[Mn^{II}_4Mn^{III}_3(OH)_3(hmp)_9Cl_3]^{3+}$ cation (hmp^- is the anion of 2-(hydroxylmethyl)-pyridine),[23,30] and the $[Mn^{II}_4Mn^{III}_3(teaH)_3(tea)_3]^{2+}$ cation (teaH = triethanolamine).[31]

Magnetic Susceptibility Studies. Variable temperature DC susceptibility measurements were performed in the 5.0−300 K range on powdered microcrystalline samples of **1**·2H_2O·$^1/_2$MeCN and **2**·2H_2O, restrained in eicosane to prevent torquing, in a 5 kG field (Figure 5). For complex **1**, the $\chi_M T$ value of 12.0 cm^3 K mol^{-1} at 300 K decreases gradually with decreasing temperature to 3.4 cm^3 K mol^{-1} at 5.0 K. For complex **2**, the $\chi_M T$ value of 12.8 cm^3 K mol^{-1} at 300 K decreases gradually to 4.1 cm^3 K mol^{-1} at 5.0 K. The spin-only value ($g = 2$) for a molecule composed of noninteracting $Mn^{III}_3Mn^{IV}_4$ ions is 16.5 cm^3 K mol^{-1}. Hence, the molecules appear to have appreciable intramolecular antiferromagnetic interactions.

Each complex contains three Mn^{III} and four Mn^{IV} centers, with total spin (*S*) values therefore ranging from 0 to 12. The low symmetry and size of the molecules make it very difficult to apply a matrix diagonalization method, and they completely preclude the application of the Kambe equivalent operator method[32] for determining the various Mn_2 pairwise exchange interaction constants (*J*) in the molecule. Efforts were instead concentrated on determining the ground-state *S* value of the complexes. Thus, magnetization data were collected in the 0.10−70 kG field and the 1.8−10.0 K temperature ranges (Figure 6). The saturation value in the highest fields is approaching the value of ∼4, which is expected for an $S = 2$ spin. However, it was not possible to obtain a reasonable fit for these data. This is likely due to the intermolecular exchange interactions mediated by the intermolecular Se···O contacts that were detected in the crystal structures and which are not incorporated in the fitting model. In addition, there may be low-lying excited states that are populated even at very low temperatures. The latter is unfortunately a common problem in higher-nuclearity clusters due to a high density of spin states and/or the presence of spin frustration effects. Spin frustration, in its general sense, is the presence of competing antiferromagnetic exchange interactions of comparable magnitude, which can often prevent (frustrate) the antiparallel alignment of all spins. Such spin frustration effects have been previously described in detail.[33] The ground-state spin values and the energies of low-lying excited states become sensitive to the precise magnitude of the competing exchange interactions. The triangular arrangement of coupled metal ions, as found in **1** and **2**, is the textbook topology for spin frustration if the couplings are antiferromagnetic since the spins cannot all be antiparallel to all of their neighbors. It is anticipated, based on the properties of dinuclear systems, that all of the oxide-bridged $Mn^{IV}Mn^{IV}$, $Mn^{IV}Mn^{III}$, and $Mn^{III}Mn^{III}$ pairwise exchange interactions in **1** and **2** will possibly be antiferromagnetic, and thus the presence of spin frustration in the cores is expected. The strongest exchange interaction within the molecule is very likely a strong antiferromagnetic

(29) Abbati, G. L.; Cornia, A.; Fabretti, A. C.; Caneschi, A.; Gatteschi, D. *Inorg. Chem.* **1998**, *37*, 3759.
(30) Bolcar, M. A.; Aubin, S. M. J.; Folting, K.; Hendrickson, D. N.; Christou, G. *Chem. Commun.* **1997**, 1485.
(31) Pilawa, B.; Kelemen, M. T.; Wanka, S.; Giesselmann, A.; Barra, A. L. *Europhys. Lett.* **1998**, *43*, 7.
(32) Kambe, K. *J. Phys. Soc. Jpn.* **1950**, *48*, 15.
(33) (a) Castro, S. L.; Sun, Z.; Grant, C. M.; Bollinger, J. C.; Hendrickson, D. N.; Christou, G. *J. Am. Chem. Soc.* **1998**, *120*, 2365. (b) Albela, B.; El Fallah, M. S.; Ribas, J.; Folting, K.; Christou, G.; Hendrickson, D. N. *Inorg. Chem.* **2001**, *40*, 1037.

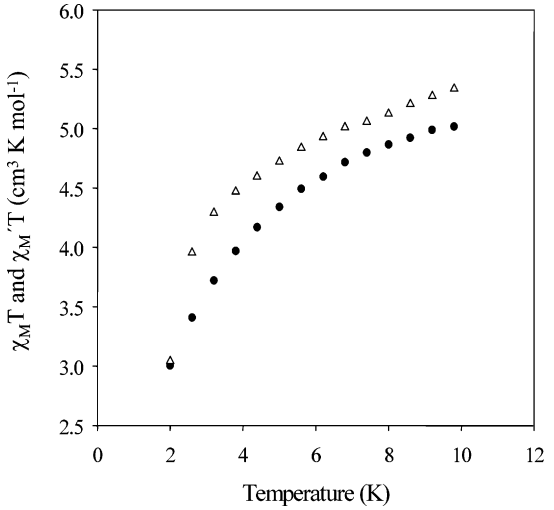

Figure 7. Plot of $\chi_M'T$ vs temperature for complex **1**·$2H_2O$·$^1/_2$MeCN in the 2.0−10.0 K range from AC magnetic susceptibility measurements (△), including the DC χ_MT data (●) from Figure 5 for this temperature range. The AC data were measured with a 3.5 G AC field oscillating at 997 Hz.

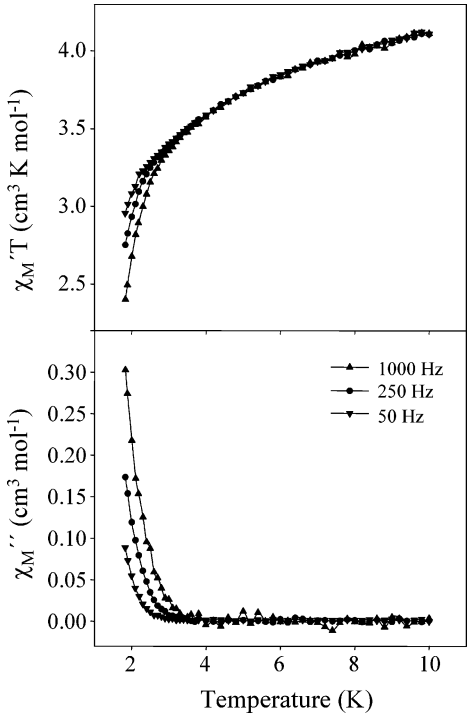

Figure 8. Out-of-phase (χ_M'') AC susceptibility signals for a dried microcrystalline sample of **1**·$2H_2O$·$^1/_2$MeCN at the indicated AC oscillation frequencies.

coupling within the Mn^{IV}_2 units. This Mn^{IV}_2 interaction in several dinuclear complexes with the $[Mn^{IV}_2(\mu\text{-}O)_2(\mu\text{-}O_2CR)]$ core is in the range from −37 to −67 cm^{-1}, depending strongly on the Mn^{IV}−O−Mn^{IV} angle,[19a,22] and it is likely that the Mn^{IV}_2 interactions in **1** and **2** are of similar magnitude. This is also the magnitude that is expected for the various $Mn^{III}Mn^{IV}$ interactions.[21]

The lowest-temperature data in Figure 5 and the saturation values of $M/N\mu_B$ in Figure 6 suggest a small ground-state spin value of $S \sim 2$ for **1**·$2H_2O$·$^1/_2$MeCN and **2**·$2H_2O$, but this is not the safest way to determine the ground-state spins because of potential complications from Zeeman effects from the applied DC field. A better way is to measure the AC susceptibility, which does not involve the use of a DC field. Such studies were carried out with a 3.5 G AC field oscillating at frequencies up to 997 Hz. In fact, the AC in-phase susceptibilities ($\chi_M'T$) for the two complexes are essentially superimposable and turn out to be very similar to the DC susceptibilities (χ_MT). The AC $\chi_M'T$ and DC χ_MT values for **1** are compared in Figure 7. The sloping $\chi_M'T$ versus T plot is strongly indicative of a population of low-lying excited states since occupation of only the ground state would give an essentially temperature-independent value. Extrapolation suggests the plot is heading to a χ_MT value of ~3 cm^3 K mol^{-1} ($S = 2$ state with $g = 2$) before a noticeable downturn is observed at the lowest temperatures due to relaxation effects (vide infra). We conclude that the ground-state spin of **1** and **2** is $S = 2$, but that there are several low-lying excited states that are significantly populated even below 10 K. Note that the extrapolation from higher temperatures also avoids complications from weak intermolecular interactions.

With such a small ground state, it seemed unlikely that complexes **1** and **2**, even with a significant magnetic anisotropy as a result of their three parallel Mn(III) elongation axes, would possess a significantly large barrier to magnetization relaxation to be SMMs. As a result, we did not expect to see an out-of-phase AC susceptibility signal (χ_M''), an indicator of slow magnetization relaxation. However, with AC oscillation frequencies up to 997 Hz (Figure 8), a frequency-dependent χ_M'' signal was indeed observed for complex **1**, or rather the tail of a χ_M'' signal whose peak lies at a temperature significantly below 1.8 K. It is very important to note that similar χ_M'' signals were seen whether we used crystals kept wet with mother liquor (i.e., **1**·6MeCN) or those that had been filtered and dried (i.e., **1**·$2H_2O$·$^1/_2$MeCN), showing that for this compound the drying and consequent change in solvation content has no significant effect on the magnetic properties. Since we did not believe **1** could be a SMM, we instead suspected that this signal might be due to a spin-chain behavior resulting from the intermolecular exchange interactions mediated by the short Se···O contacts observed in the crystal structure. We thus decided to investigate the magnetic properties at lower temperatures.

DC Magnetization Studies below 1.8 K. Single-molecule magnets (SMMs) or single-chain magnets (SCMs)[34−38] below their blocking temperature, T_B, will exhibit hysteresis in their

(34) Clérac, R.; Miyasaka, H.; Yamashita, M.; Coulon, C. *J. Am. Chem. Soc.* **2002**, *124*, 12837.
(35) Miyasaka, H.; Clérac, R.; Mizushima, K.; Sugiura, K.; Yamashita, M.; Wernsdorfer, W.; Coulon, C. *Inorg. Chem.* **2003**, *42*, 8203.
(36) (a) Caneschi, A.; Gatteschi, D.; Lalioti, N.; Sangregorio, C.; Sessoli, R.; Venturi, G.; Vindigni, A.; Rettori, A.; Pini, M. G.; Novak, M. A. *Angew. Chem., Int. Ed.* **2001**, *40*, 1760. (b) Caneschi, A.; Gatteschi, D.; Lalioti, N.; Sessoli, R.; Sorace, L.; Tangoulis, V.; Vindigni, A. *Chem.—Eur. J.* **2002**, *8*, 286. (c) Caneschi, A.; Gatteschi, D.; Lalioti, N.; Sangregorio, C.; Sessoli, R.; Venturi, G.; Vindigni, A.; Rettori, A.; Pini, M. G.; Novak, M. A. *Europhys. Lett.* **2002**, *58*, 771.
(37) (a) Liu, T.-F.; Fu, D.; Gao, S.; Zhang, Y.-Z.; Sun, H.-L.; Su, G.; Liu, Y.-J. *J. Am. Chem. Soc.* **2003**, *125*, 13976. (b) Shaikh, N.; Panja, A.; Goswami, S.; Banerjee, P.; Vojtíek, P.; Zhang, Y.-Z.; Su, G.; Gao, S. *Inorg. Chem.* **2004**, *43*, 849.

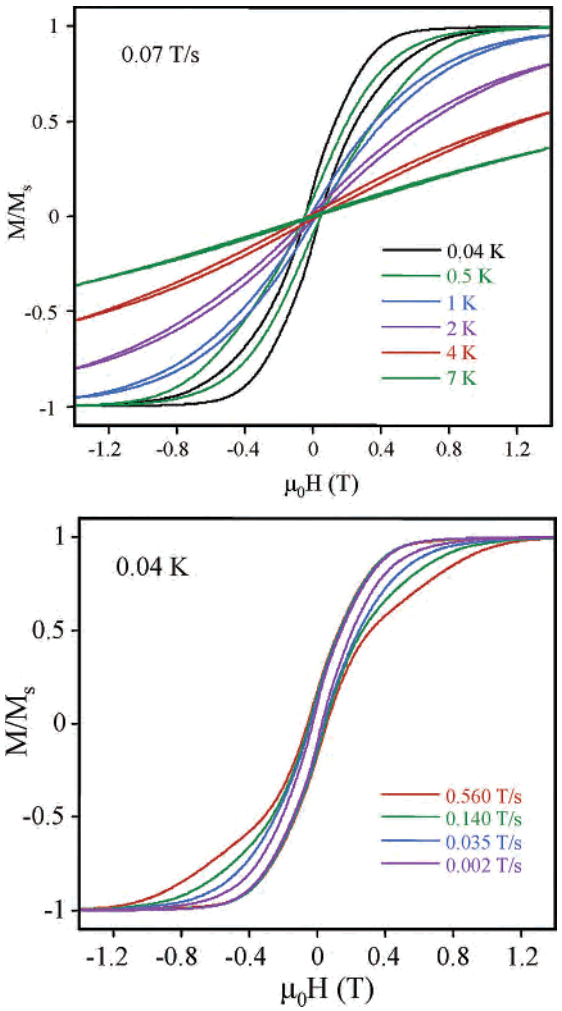

Figure 9. Magnetization vs DC field plots for a single crystal of complex **1**·6MeCN (top) at the indicated temperatures and a fixed field-sweep rate of 0.07 T/s and four sweep rates (bottom) at a fixed temperature of 0.04 K. The magnetization is normalized to its maximum value, M_s.

magnetization versus DC field response, which is the classical property of a magnet. Such studies were therefore performed on a single crystal of **1**·6MeCN using a micro-SQUID apparatus;[13] crystals were kept wet with mother liquor to prevent any damage from the loss of solvent. Measurements were performed in the 0.04−7.0 K temperature range, using different field sweep rates from 0.008 to 0.56 T/s. The sensitivity and time resolution of a micro-SQUID magnetometer allow the study of very small single crystals in good contact with a thermal bath. The temperature dependence at a fixed sweep rate of 0.07 T/s is shown in Figure 9 (top panel). Hysteresis loops become evident in the scans at 4 K, but they only have a small coercivity. The latter increases, but only slightly, with decreasing temperature down to 0.5 K and then is constant down to 0.04 K. Figure 9 (bottom panel) shows the sweep-rate dependence of the loops at a constant temperature of 0.04 K. A small decrease

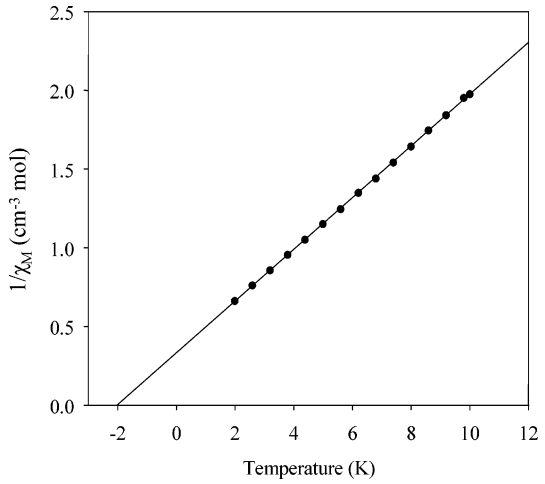

Figure 10. Curie−Weiss plot for **1**·2H$_2$O·$^1/_2$MeCN showing a negative (antiferromagnetic) intercept assigned to interchain interactions.

in coercivity is observed with a decreasing sweep rate, but again, the change is only slight. This behavior is *not* that expected for an SMM, for which one would expect a greater dependence of the coercivity on the temperature and on the sweep rate. Instead, we believe that the hysteresis behavior is the consequence of the one-dimensional chain structures of **1** and **2** in the solid state. Thus, complex **1** (and by implication, **2**, given its very similar structure) appears to be a new example of the small but growing family of single-chain magnets (SCMs).[39] This implies that the intermolecular interactions mediated by the Se···O contacts are ferromagnetic in nature, leading to a parallel alignment of spins of the interacting Mn_7 units along the chain, a significant barrier (versus thermal energy) to magnetization reversal, and the resulting hysteresis loops.

However, closer inspection of the loops in Figure 9 indicates that this ferromagnetic coupling between molecules within the chains is not sufficient to completely account for the observed hysteresis behavior. Following saturation of the magnetization in one direction with a large field, the reversal of the direction of the magnetization should occur after the field has been swept past zero for a ferromagnetically coupled chain. However, this is clearly not the case in Figure 9; the reversal of the magnetization direction begins before the zero field. This feature is characteristic of the presence of antiferromagnetic interactions, and we identify these as interchain interactions mediated by the weak contacts observed in the crystal structure. Similar behavior has been observed in some SMM systems, including $[CeMn_8O_8(O_2CMe)_{12}(H_2O)_4]$[40] and the Fe_{19} SMMs.[41]

Since the hysteresis loops are suggestive of antiferromagnetic interchain interactions, we sought additional evidence for their presence, and this was obtained from the Curie−Weiss plot of the lowest-temperature DC susceptibility data (shown in Figure 10). The Weiss constant is obtained from the *x*-axis intercept (−2.0 K), confirming the weakest

(38) (a) Lescouëzec, R.; Vaissermann, J.; Ruiz-Pérez, C.; Lloret, F.; Carrasco, R.; Julve, M.; Verdaguer, M.; Dromzee, Y.; Gatteschi, D.; Wernsdorfer, W. *Angew. Chem., Int. Ed.* **2003**, *42*, 1483. (b) Toma, L. M.; Lescouëzec, R.; Lloret, F.; Julve, M.; Vaissermann, J.; Verdaguer, M. *Chem. Commun.* **2003**, *15*, 1850.

(39) Glauber, R. J. *J. Math. Phys.* **1963**, *4*, 294.

(40) Tasiopoulos, A. J.; Wernsdorfer, W.; Moulton, B.; Zaworotko, M. J.; Christou, G. *J. Am. Chem. Soc.* **2003**, *125*, 15274.

(41) Goodwin, J. C.; Sessoli, R.; Gatteschi, D.; Wernsdorfer, W.; Powell, A. K.; Heath, S. L. *J. Chem. Soc., Dalton Trans.* **2000**, *12*, 1835.

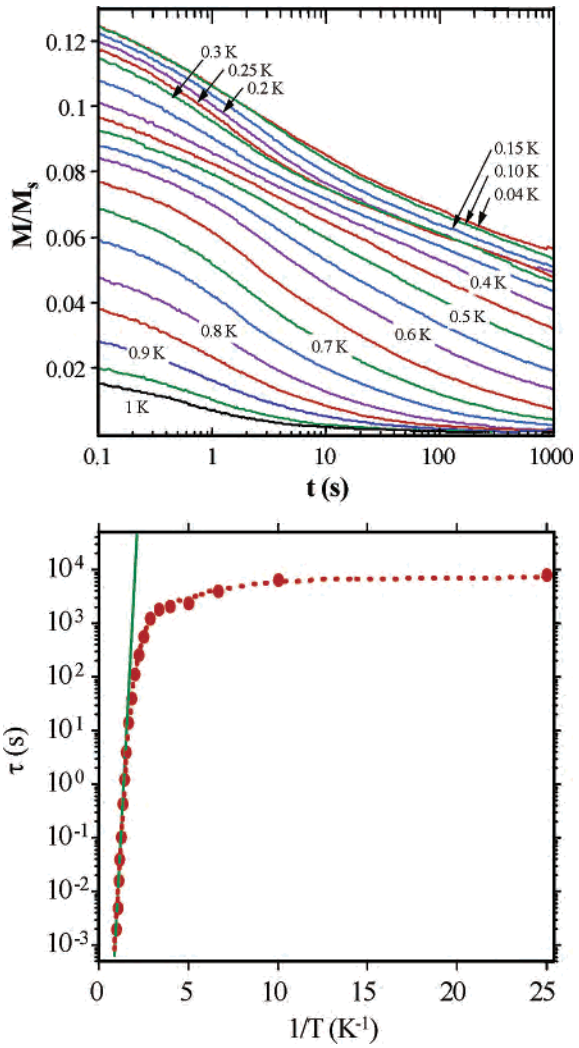

Figure 11. Magnetization vs time decay plots (top) for a single crystal of **1**·6MeCN at the indicated temperatures. Arrhenius plot (bottom) using the resulting relaxation lifetime (τ) vs T data. The green line is a fit of the thermally activated region to the Arrhenius equation. See the text for the fit values.

interaction in the system to be antiferromagnetic. This is assigned to the interchain interaction.

To characterize the system further, we collected magnetization decay data to determine the barrier to magnetization relaxation. The magnetization of the sample was saturated in one direction with a large applied field at 5 K. The temperature was decreased to a chosen value in the 0.04−1.0 K range. The applied field was removed, and the magnetization of the sample was monitored with time. The resulting data are shown in Figure 11 (top panel). The decay data at each temperature were analyzed to give a set of relaxation time (τ) versus temperature data, which were used to construct the Arrhenius plot of Figure 11 (bottom panel), based on the Arrhenius relationship of eq 2, where τ_0 is the preexponential factor, U_{eff} is the mean effective barrier to relaxation, and k is the Boltzmann constant.

$$\tau = \tau_0 \exp(U_{eff}/kT) \qquad (2)$$

The fit of the thermally activated region above ~0.5 K (shown as the green line in Figure 11 (bottom panel)) gave $U_{eff} = 9.87\ cm^{-1} = 14.2$ K and $1/\tau_0 = 1.9 \times 10^{-9}\ s^{-1}$. Below this temperature, the relaxation time levels off and becomes temperature-independent at ~10^4 s. This temperature independence of the relaxation rate is the characteristic signature of quantum tunneling of the magnetization through the anisotropy barrier.

Origin of the Relaxation Barrier. The picture that emerges from the above magnetic analysis of complex **1** is that there is a significant barrier to magnetization relaxation of 14.2 K in this compound. As a result, at low temperatures, the compound exhibits the characteristic behavior of a magnet, namely, magnetization hysteresis. This cannot be rationalized on the basis of single-molecule magnetism because the spin of the molecule is only $S = 2$, and this is unlikely to give a significant barrier to magnetization relaxation. The upper limit (U) of the latter for an integer spin system is given by $U = S^2|D|$, where D is the axial anisotropy (zero-field splitting) parameter. Even assuming a value of $D = -1.0\ cm^{-1}$, which is actually larger (more negative) than is typical for Mn_x clusters, would still only give a barrier U of 4.0 cm^{-1} (5.8 K). When one then takes into account that the actual (or effective) barrier (U_{eff}) is usually considerably less than U, because the magnetization can tunnel through the barrier via higher-lying M_S levels rather than going over the top, then it becomes impossible to convincingly rationalize the observed effective barrier (U_{eff}) of 9.87 cm^{-1} = 14.2 K on the basis of the properties of the individual molecules of **1**.

Instead, as we mentioned earlier, we interpret the observed behavior as a result of the one-dimensional chains formed between Mn_7 molecules, giving a single-chain magnet (SCM). The latter is a relatively new phenomenon in molecular magnetism, but it is nevertheless now well-established with several well-documented examples.[34−38] In such a system, the magnetization relaxation barrier and the resulting slow relaxation rates are caused by one-dimensional intermolecular exchange interactions between the constituent spin carriers. Such chains may be either homometallic[37] or heterometallic[35,38] and can even comprise an alternating metal/organic radical arrangement.[36] According to the Glauber theory for one-dimensional Ising chains,[39] the magnetization relaxation rate follows an Arrhenius law (eq 3) with a barrier given by $8JS^2$ (for the $-2J\hat{S}_i\cdot\hat{S}_j$ convention), where S is the spin of the repeating unit and J is the exchange parameter between these units.

$$\tau = \tau_0 \exp(8JS^2/kT) \qquad (3)$$

If the repeating unit also possesses an intrinsic anisotropy and thus a magnetization relaxation barrier of $U = S^2|D|$, then there will be two contributions to the total relaxation barrier: that from the anisotropy of the molecular unit and that from the interaction between these units. This was clearly described in a recent paper by Miyasaka et al. on a series of related SCMs,[35] and the corresponding Arrhenius relationship for such a system can then be expressed by eq 4

$$\tau = \tau_0 \exp(\Delta/kT) \qquad (4)$$

where $\Delta = (8J + |D|)S^2$ is the barrier to magnetization relaxation, or rather its upper limit in the absence of tunneling.

The results described in the present work can be rationalized within the framework of the above model. The Mn_7 cluster has a small but nevertheless significant spin of $S = 2$, and in the presence of some easy axis (or Ising) type anisotropy, as expected for axially elongated Mn(III), there will be a small barrier to magnetization relaxation. This is insufficient for providing a single-molecule magnet, but the interactions between the Mn_7 units (Figure 3) provide an additional contribution to the barrier. As a result, and even if one allows for the diminution of the barrier by tunneling effects, there is still a large enough barrier (U_{eff}) of 14.2 K to yield out-of-phase AC susceptibility signals and hysteresis.

The relaxation barrier for complex **1** of 14.2 K is unfortunately rather small compared with those of other SCMs in the literature, which fall in the range of 50−154 K.[34−38] In addition, there are noticeable interchain interactions; so, the best description of **1** is as an SCM with weak interchain coupling, in the same way that SMMs with weak intermolecular interactions are also known.[40,41] The important thing is that in these SMMs, and also complex **1**, the intermolecular or interchain interactions are weak enough to be considered a perturbation of the SMM or SCM behavior, respectively, rather than strong enough to give a true three-dimensional ordered solid. Clearly, the frequency-dependent AC data and the sweep rate and temperature-dependent coercivities in the hysteresis loops rule out **1** as a three-dimensional magnet. Thus, regardless of its low anisotropy barrier, it is appropriate to call **1** a SCM. It would also be the first example to consist of a chain of polynuclear metal clusters rather than mononuclear or dinuclear repeating units, and it is also the first to exhibit the temperature-independent relaxation regime in the Arrhenius plot characteristic of quantum tunneling. It thus represents a significant new addition to the SCM family.

Conclusions

The use of benzeneseleninic acid ($PhSeO_2H$) in attempted ligand-substitution reactions with $[Mn_{12}O_{12}(O_2CMe)_{16}(H_2O)_4]$ (**3**) causes a structural change and has afforded two new heptanuclear Mn clusters, $[Mn_7O_8(O_2SePh)_8(O_2CMe)(H_2O)]$ (**1**) and $[Mn_7O_8(O_2SePh)_9(H_2O)]$ (**2**), which possess a novel $[Mn^{III}_3Mn^{IV}_4(\mu_3\text{-}O)_5(\mu\text{-}O)_3]^{9+}$ core and represent the first examples of transition-metal clusters ligated by $PhSeO_2^-$ groups. Magnetic studies suggest a low ground-state spin value of $S = 2$ and the appearance in the AC susceptibility of out-of-phase signals characteristic of slow magnetization relaxation. Studies down to 0.04 K reveal that these species are not new additions to the growing family of single-molecule magnets (SMMs). Instead, the slow relaxation is caused by single-chain magnetism behavior, with the relaxation barrier arising from a combination of the molecular anisotropy and the exchange interaction between the individual Mn_7 molecules. These complexes are thus interesting for a number of reasons, including aesthetically pleasing structures and their average oxidation state of +3.6, which is unusually high for a high-nuclearity Mn cluster. It will be interesting to see in future work whether the $PhSeO_2^-$ allows access to other high-oxidation-state species.

Finally, it is important to remember for the future that the observation of the χ_M'' signals in Figure 8 for an ostensibly molecular compound did not presage the observation of the characteristic properties of a SMM. This represents an important reminder that it is not safe to take the appearance of χ_M'' signals as sufficient proof that a SMM has been prepared.

Acknowledgment. This work was supported by the National Science Foundation.

Supporting Information Available: X-ray crystallographic files in CIF format for complexes **1**·6MeCN and **2**·$2CH_2Cl_2$. This material is available free of charge via the Internet at http://pubs.acs.org.

IC0494049